Bi-Hierarchy Capacity Programming of Co-phase TPSS With PV and HESS for Minimum Life Cycle Cost

Minwu Chen[a], Xin Gong[a,*], Zongyou Liang[a], Jinyu Zhao[a], Zhongbei Tian[b]

[a]*School of Electrical Engineering, Southwest Jiaotong University, Chengdu 611756, China*
[b]*School of Electrical Engineering and Electronics, The University of Liverpool, Liverpool L69 3BX, United Kingdom*
***** Correspondence: gong_x@my.swjtu.edu.cn;

Abstract: Co-phase traction power supply system (TPSS) with photovoltaic (PV) and hybrid energy storage system (HESS) is a promising way to improve the utilization of regenerative braking energy (RBE) and power quality. However, despite co-phase TPSS with PV and HESS being beneficial from the perspective of technology, how to coordinate the operation strategies of various devices to ensure system economy is a key issue in practical engineering applications. Therefore, this paper proposes a bi-hierarchy capacity programming strategy of co-phase TPSS to minimize life cycle cost. In the upper layer, the integrated lifetime evaluation model of HESS and PFC (HESS-PFC) is proposed for the lower long-term investment cost. Remarkably, the PFC reliability assessment and the HESS degradation process are analyzed. Meanwhile, the capacity of HESS-PFC is obtained, and the lifetime of HESS-PFC is extended. In the lower layer, the power flow of co-phase TPSS is optimized to minimize short-term operating cost under satisfying three-phase voltage unbalance standards. Traction load peak-shaving and valley-filling are achieved by coordinating HESS-PFC and PV. And it is formulated as a mixed integer linear programming model based on efficient linearization methods. Whale optimization algorithm with GUROBI solver embedded is employed to solve this bi-hierarchy model. Finally, case studies show that the proposed model can achieve 23.26% cost reduction and 63.82% PFC lifetime extension, while the voltage unbalance is within an allowable range of 2%.

Keywords: Co-phase traction power supply system; hybrid energy storage system; power flow controller; life cycle cost

Nomenclature

A. Abbreviations, Indices and Suffixes

TPSS	Traction power supply system
HESS	Hybrid energy storage system
PV	Photovoltaic
RBE	Regenerative braking energy
PFC	Power flow controller
LCC	Life cycle cost
MILP	Mixed integer linear programming
UC	Ultracapacitor
WOA	Whale optimization algorithm
t, Δt	Time index and interval
s	PV scenario sets

B. Parameters

$Z_{\mathrm{js.T/D}}$	Thermal impedance of between module junction and heatsink of IGBT/Diode
Z_{sa}	Thermal impedance of between heatsink and ambient
T_{jmax}, T_{jmin}	Maximum and minimum junction temperature for the jth thermal cycle
u, T_{MTTR}	Repair rate and mean time to repair of PFC
CRF, SFF	Capital recovery factor and sinking fund factor
r	Interest rate
T_{proj}	Project period (20 year in this paper)
$k_{b/ue}$, $k_{b/up}$	Unit capacity and power cost of battery and UC
k_{bop}	Auxiliary equipment cost per unit
k_p	PFC capital cost per unit installed capacity
$k_{bo.f}$, $k_{bo.v}$	Battery fixed and variable cost per unit
k_{br}	Battery replacement cost per unit
T_p	PFC annual operating hours
C_{lt}	PFC labor and travel cost per repair
κ_1	PFC investment cost coefficient
κ_2, κ_3	Depreciation coefficient for the recovery of battery and PFC
N_{T}	Total number of time intervals in a day (=1440)
π_s	Probability value of PV related scenario
$\rho_{t,s}^{\mathrm{grid}}$	Price of purchased electricity from power grid
$\rho_{t,s}^{\mathrm{dem}}$	Demand power electricity price per unit
$\rho_{t,s}^{\mathrm{fed}}$	Price of electricity fed back to power grid
$\rho_{t,s}^{\mathrm{PV}}$	Daily O&M costs of PV per unit
$P_{t,s}^{\mathrm{LD}}$, $P_{t,s}^{\mathrm{RBE}}$	Active power of train traction and braking
$Q_{t,s}^{\mathrm{LD}}$, $Q_{t,s}^{\mathrm{RBE}}$	Reactive power of train traction and braking
$\eta_{\mathrm{ch}}^{\mathrm{b/u}}$, $\eta_{\mathrm{dis}}^{\mathrm{b/u}}$	Charge/discharge-efficiency of battery and UC
$SOC_{\mathrm{min/max}}^{\mathrm{b/u}}$	Max-limits and min-limits of battery and UC
$SOC_{\mathrm{t=0}}^{\mathrm{b/u}}$	Initial SOC of battery and UC
ε_{b}, ε_{u}	Self-discharge rate of the battery and UC
φ_{T}, φ_{α}	Power factor angles of TT and α-phase of PFC

C. Optimization Variables

$P_{t,s}^{\mathrm{dem}}$, $P_{t,s}^{\mathrm{peak}}$	Demand power and its maximum peak
$P_{t,s}^{\mathrm{T}}$, $P_{t,s}^{\mathrm{PV}}$	Active power of TT and PV
$P_{t,s}^{\alpha}$, $P_{t,s}^{\beta}$	Active power of α and β-converters
$P_{t,s}^{\mathrm{b/u,dis}}$, $P_{t,s}^{\mathrm{b/u,ch}}$	Discharge and charge power of battery and UC
$E_{t,s}^{\mathrm{b/u}}$	The energy stored in battery and UC
$P_{t,s}^{\mathrm{grid.max}}$	Maximum interactive power with the grid
$Q_{t,s}^{\alpha}$, $Q_{t,s}^{\beta}$	Reactive power of α and β-converters
λ, T_{MTTF}	Failure rate and mean time to failure of PFC
T_b, T_{bh}	Battery lifetime and daily operating hours
N_R	Battery replacement number
$P_{\mathrm{r}}^{\mathrm{b/u}}$, $E_{\mathrm{r}}^{\mathrm{b/u}}$	Rated power and capacity of battery and UC
S_{PFC}	Rated capacity of PFC

1. Introduction

With the continuous expansion of electrified railway mileage in recent decades, the eco-friendly and energy-efficient operation of traction power supply systems (TPSS) has raised significant concerns [1,2]. The rapid development of renewable energy and hybrid energy storage systems (HESS) provides an effective solution for railway energy saving and cost reduction [3].

On the one hand, renewable energy along railway lines is used to reduce short-term operating cost. References [4, 5] provide the application prospect for photovoltaics (PV) and regenerative braking energy (RBE) utilization in TPSS. On the other hand, different energy storage systems are installed in TPSS, which is also a potential way. In [6, 7], HESS consisting of battery and ultracapacitor (UC) are a promising solution to recycle RBE and reduce operating cost. In the above references, PV and HESS are directly connected to the traction network through converters, which may lead to power quality problems, such as network voltage fluctuation [8]. In addition, the distribution of HESS and PV along the railway results in expensive operation and maintenance costs [7]. The proposed co-phase TPSS can provide a flexible interface for PV and HESS, which consists of single-phase traction transformers (TT) and power flow controllers (PFC) [9].

As the core component of co-phase TPSS, PFC adopts high-voltage and large-capacity converter technology to achieve negative sequence compensation and promote the high-efficient utilization of energy. Its lifetime is mainly determined by the reliability of insulated gate bipolar transistors (IGBT) and freewheeling diodes [10]. Junction temperature management is an effective method to improve the reliability of the converter [11]. In [12], a control strategy is proposed to promote PFC reliability and prolong the PFC lifetime by 16.28%. However, when PV and HESS are connected to PFC, the above research methods need to be improved. As a result, it is necessary to propose an integrated lifetime evaluation model of HESS and PFC (HESS-PFC).

It is widely accepted that HESS capacity is one of the critical issues that affect system economics. The programming approaches of capacity sizing for HESS are extensively applied in other fields, such as microgrids [13], household-prosumers [14, 15], EVs [16], and so on. The optimal sizing and power management of PV and HESS are studied in [14]. These references provide inspiration for capacity programming of railway systems. In [17], a mixed integer linear programming (MILP) model is presented to optimize the HESS sizing for RBE utilization. Reference [7] employs a bi-level model of railway energy management systems to optimize the HESS sizing and the grey wolf algorithm is employed. But the three-phase voltage unbalance is neglected, which is an important index to assess the power quality of TPSS. Besides, in the co-phase TPSS, additional investment of the PFC is essential, so it is meaningful to optimize the PFC capacity. In [18], a life cycle cost (LCC) model of the PFC is built to determine the PFC capacity. However, few publications are associated with the optimal scheduling and capacity programming of HESS-PFC.

A detailed comparison of the above studies in the objectives, methods and results is given in Table I. Accordingly, this paper presents a comprehensive approach to planning the HESS-PFC capacity and optimizing the co-phase TPSS operation for minimum life cycle cost, which meets the standard limit of three-phase voltage unbalance, prolongs PFC and battery lifetime, and realizes the economy of the capacity planning. The highlights of this paper can be outlined as follows:

1) A scheduling optimization model for co-phase TPSS with PV and HESS is proposed, which takes the three-phase voltage unbalance as the constraint and short-term operating cost as the objective. It can sufficiently coordinate HESS-PFC and PV to achieve traction load peak-shaving and valley-filling and improve power quality comprehensively.
2) Considering the interactive influence of PFC reliability and HESS charge/discharge, an integrated lifetime evaluation model of HESS-PFC is established. The PFC reliability assessment and battery degradation process are embedded into the model to evaluate the PFC and battery lifetime for the lower long-term investment cost.

Table 1
Comparisons among aforementioned studies and this paper

Reference	Objectives				Methods				Results	
	Utilize RBE	Remove NS	Solve VU	Save cost	Bi-level model	System electronics	TOU policy	Solution method	Optimize sizing	Prolong lifetime
[2, 20]	√	×	√	√	×	RPC	×	PSO	√	×
[3]	√	√	√	×	√	PFC	√	CPLEX	×	×
[4, 5]	√	×	×	√	×	×	×	/	√	×
[6]	√	×	×	×	√	×	×	HC	×	×
[8]	√	×	×	√	√	×	√	GWO	√	√
[10, 12]	×	×	×	×	×	PFC	×	PSO	×	√
[13]	×	×	×	√	×	×	√	DE	×	√
[14-15]	√	×	×	×	×	×	×	TLBO	√	×
[16]	×	×	×	√	×	×	×	WOA	×	×
[17]	√	×	×	√	×	×	√	CPLEX	√	×
[18]	×	×	×	√	×	PFC	×	PSO	√	√
[19]	×	×	×	√	√	×	√	GUROBI	√	√
This paper	√	√	√	√	√	PFC	√	WOA	√	√

Note that: RBE-Regenerative braking energy; NS-Neutral sections; VU-Voltage unbalance; RPC-Railway static power conditioner; PFC-Power flow controller; PSO-Particle swarm optimization; DE-Differential evolutionary; TLBO-Teaching-learning based optimization; GWO-Grey wolf optimization; WOA-Whale optimization algorithm.

3) A bi-hierarchy capacity programming strategy is designed to combine long-term investment cost and short-term operating cost for achieving minimize life cycle cost. In the upper layer, the capacity of HESS-PFC as the input of the lower layer is planned. In the lower layer, the optimization scheduling results is fed back to the upper layer. A globally optimal solution is obtained through multiple iterations.

The rest of this paper is structured as follows. Section II introduces the system description. Section III presents the upper layer capacity programming model. The lower layer scheduling optimization model is developed in Section IV. In Section V, WOA with GUROBI solver embedded is applied for problem solving. In Section VI, case studies are presented and the conclusion is reached in Section VII.

2. System description

Fig. 1 shows the structure of co-phase TPSS with PV and HESS. The co-phase TPSS proposed in this paper mainly consisted of single-phase TT and PFC, PV, and HESS. In this structure, the combination of single-phase TT and PFC can cancel the neutral section and provide continuous supply power for trains without any obstacle. PFC is the key component of co-phase TPSS, which is composed of multiple high-voltage and large-capacity back-to-back connected converters. The direct-current link of the PFC provides a favorable interface for PV and HESS. The connection of PV can improve the utilization rate of renewable energy. Considering stochastic fluctuations of traction load and PV uncertainty, HESS composing of battery and UC is selected as the storage medium for TPSS. The combination of the two is more conducive to promoting the RBE utilization of the railway system and improving the operating efficiency of the system.

Fig. 2 illustrates the block diagram of the bi-hierarchy capacity programming strategy proposed in this paper. The bi-hierarchy strategy of co-phase TPSS with PV and HESS includes the upper layer capacity programming model and the lower layer optimal scheduling model. And three goals are achieved: i) minimize the LCC of co-phase TPSS, ii) meet the power quality standard with

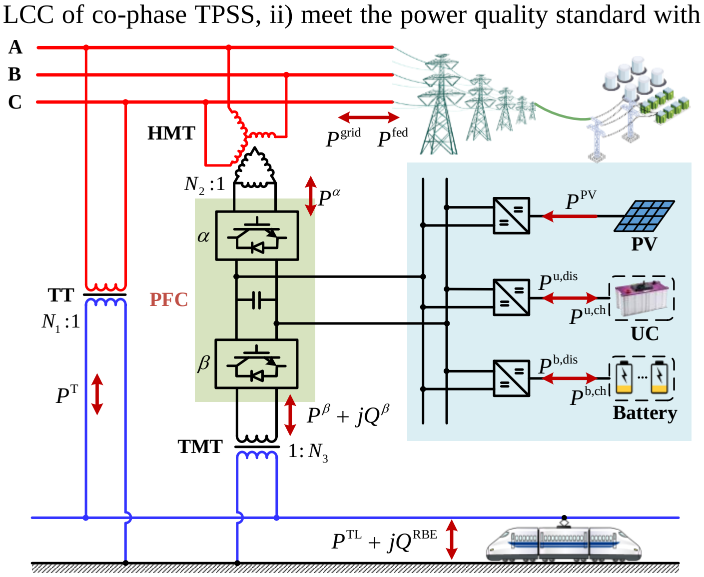

HMT-High-voltage matching transformer; TMT-Traction matching transformer.
Fig. 1. Structure of co-phase TPSS with PV and HESS.

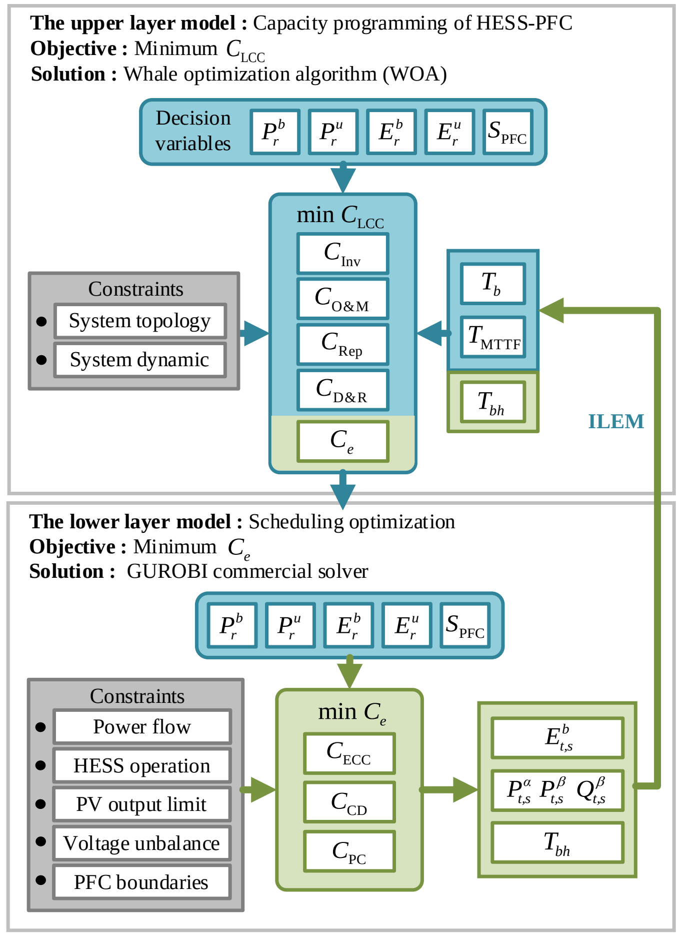

Note that: ILEM-Integrated lifetime evaluation model.
Fig. 2. Block diagram of bi-hierarchy capacity programming strategy proposed.

three-phase voltage unbalance, and iii) prolong battery and PFC lifetime. In the upper layer model, taking the battery and PFC lifetime into account, the co-phase TPSS capacity-optimized and LCC-calculated are implemented. The capacity configuration of HESS-PFC is obtained from the upper layer and as input of the optimal scheduling model. In the lower layer, the optimal HESS scheduling strategy and PFC compensation power are obtained under satisfying negative sequence requirements with the goal of minimum short-term operating cost. Then, the lower layer results are fed back to the upper layer. Therefore, the proposed bi-hierarchy capacity programming strategy can combine long-term investment cost and short-term operating cost. The minimum LCC and optimal capacity of HESS-PFC are obtained through multiple iterations.

3. Upper layer: Capacity programming model

3.1. Integrated lifetime evaluation model of HESS-PFC

Fig. 3 presents that the integrated lifetime evaluation model (ILEM) of HESS-PFC is developed to accurately calculate the lifetime of HESS-PFC, including PFC reliability assessment and HESS degradation process. The input parameters of lifetime evaluation are fed back from the lower layer, therefore, ILEM embedded in the upper layer can provide a bridge between long-term programming and short-term operations.

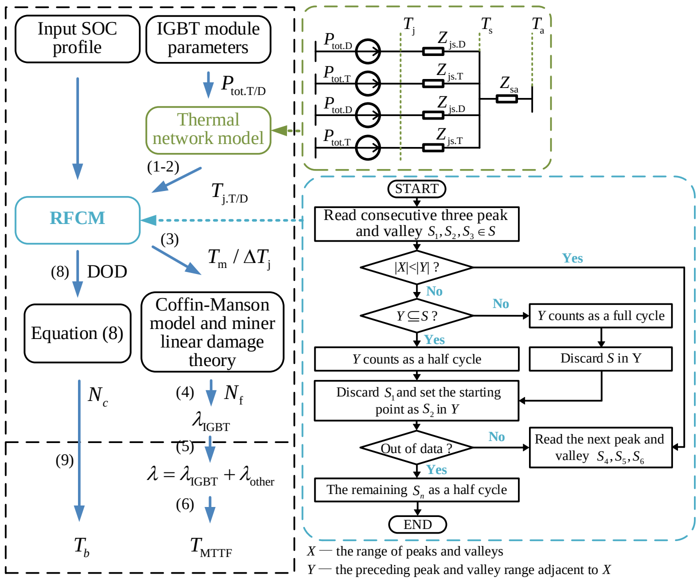

RFCM- Rain-flow counting method.

Fig. 3. Integrated lifetime evaluation model of HESS-PFC.

3.1.1 PFC reliability assessment

The topological structure of PFC is shown in Fig. 4. The IGBT modules are the main cause of PFC failure. The main reason for converters failure is the aging of the device caused by the uneven thermal stress between the materials of each layer caused by random thermal cycling [10]. The process is “two lines and four steps”. Two lines mean that the failure rate of IGBT module λ_{IGBT} is calculated based on the physical failure mechanism, and the failure rate of other components λ_{other} (such as direct-current support capacitors λ_{C}, series reactors λ_{L}, control panels λ_{D}) is gained directly based on reliability manual [12].

The reliability evaluation of IGBT modules is divided into four steps: First, power loss ($P_{\text{tot.T}}$, $P_{\text{tot.D}}$) is calculated and got according to the compensation power optimized by the lower layer. Second, junction temperature ($T_{\text{j.T}}$, $T_{\text{j.D}}$) is evaluated through established thermal network model.

$$T_{\text{j.T}} = P_{\text{tot.T}} Z_{\text{js.T}} + (P_{\text{tot.T}} + P_{\text{tot.D}}) Z_{\text{sa}} \tag{1}$$

$$T_{\text{j.D}} = P_{\text{tot.D}} Z_{\text{js.D}} + (P_{\text{tot.T}} + P_{\text{tot.D}}) Z_{\text{sa}} \tag{2}$$

Third, based on RFCM, T_{m} and ΔT_{j} of each thermal cycle are obtained in (3). Fourth, the number of cycles to failure N_{f} (ΔT_{j} , T_{m}) at T_{m} and ΔT_{j} is determined based on Coffin-Manson model in (4), a and n are adjustment parameters, a=302500, n=5.039. E_{a} is the activation energy constant, 9.891×10^{20} J, k is the Boltzmann constant, 1.38×10^{-23} J/K, thus λ_{IGBT} is obtained based on the miner linear damage theory, where $N(\Delta T_{\text{j}}, T_{\text{m}})$ is the number of thermal cycles corresponding to T_{m} and ΔT_{j} in T. Therefore, PFC failure rate λ is expressed in (5).

$$T_{\text{m}} = (T_{\text{jmax}} + T_{\text{jmin}})/2\,, \quad \Delta T_{\text{j}} = T_{\text{jmax}} - T_{\text{jmin}} \tag{3}$$

$$N_{\text{f}}\left(\Delta T_{\text{j}}, T_{\text{m}}\right) = a \cdot \left(\Delta T_{\text{j}}\right)^{-n} \cdot \exp\left[E_{\text{a}} / \left(k \cdot T_{\text{m}}\right)\right] \tag{4}$$

$$\lambda = \lambda_{\text{IGBT}} + \lambda_{\text{other}} = \int_0^T \frac{N(\Delta T_{\text{j}}, T_{\text{m}})}{N_{\text{f}}(\Delta T_{\text{j}}, T_{\text{m}})} + \left(\lambda_{\text{C}} + \lambda_{\text{L}} + \lambda_{\text{D}}\right) \tag{5}$$

In addition, the mean time to failure (T_{MTTF}) and the mean time to repair (T_{MTTR}) is respectively the mean uptime and the mean downtime of PFC, is calculated by (6).

$$T_{\text{MTTF}} = \frac{1}{\lambda}\,, \quad T_{\text{MTTR}} = \frac{1}{u} \tag{6}$$

Considering two converters of PFC share a common direct-current link, their capacities (S_α and S_β) should be equal [2]. Therefore, PFC capacity S_{PFC} can be derived as.

$$S_{\text{PFC}} = 2 \times \max\left\{S_\alpha, S_\beta\right\} \tag{7}$$

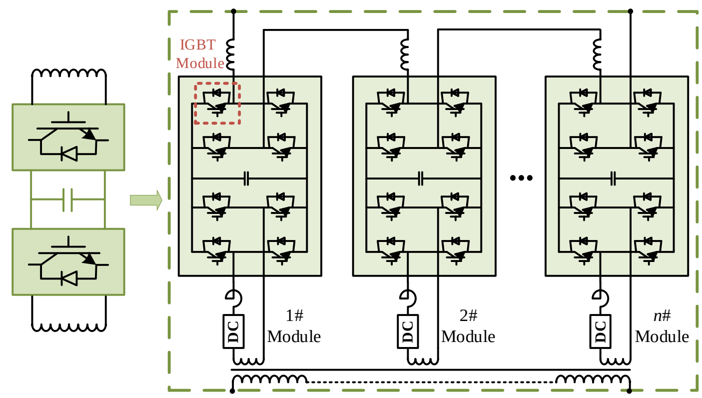

Fig. 4. The topological structure of power flow controller.

3.1.2 Battery degradation process

The HESS lifetime is affected by the shock and sharp fluctuation of traction load. The UC lifetime is mostly affected by temperature, discharge rate and terminal voltage [19]. Furthermore, the charging and discharging rates have little effect on UC lifetime, and its cycle times are as high as 500,000 ~1000,000 times and far exceeding that of batteries [17]. Hence, this paper mainly considers the battery lifetime, which is related to the number of discharge-charge cycles and the depth of discharge (DOD). The cycle counting method [20] is adopted to calculate the battery lifetime. The calculation steps are: 1) Take the battery SOC curve obtained through the optimization of the lower layer model as the known input. 2) The cycle counting model is used to extract a series of full cycles and half cycles, and calculate DOD of the corresponding cycles. 3) Eq. (8) expresses the relationship between the number of battery cycles (N_c) and DOD fitted by the least square method based on the manufacturer’s data. 4) The battery lifetime is obtained, as (9).

$$N_c\left(\text{DOD}\right) = 24090e^{-9.346\text{DOD}} + 6085e^{-1.319\text{DOD}} \tag{8}$$

$$T_b = \frac{1}{365 \cdot \sum_{i=1}^{N} \dfrac{1}{N_c\left(\text{DOD}_i\right)}} \tag{9}$$

3.2. Life cycle cost of co-phase TPSS with PV and HESS

3.2.1 Investment cost

HESS mainly include battery, UC and balance of plant (BOP) costs C_{hi}. The investment cost of PFC C_{pi} is determined by its installed capacity. Therefore, the investment cost C_{Inv} of co-phase TPSS is presented as (10).

$$C_{\text{Inv}} = C_{hi} + C_{pi} \tag{10}$$

where:

$$C_{hi} = \frac{1}{365} \cdot \left[k_{be} E_r^b + k_{ue} E_r^u + k_{bp} P_r^b + k_{up} P_r^u + k_{bop} \left(P_r^b + P_r^u \right) \right] \quad (11)$$

$$C_{pi} = \frac{1}{365} \cdot k_{\text{PFC}} \cdot S_{\text{PFC}} \quad (12)$$

3.2.2 Operation and maintenance (O&M) cost

The O&M cost of co-phase TPSS $C_{\text{O\&M}}$ can be given by the accumulation of HESS O&M cost C_{hm}, PFC operation loss cost C_{ps} and maintenance cost C_{pm}, as well as PV O&M cost C_{PV}, as (13).

$$C_{\text{O\&M}} = C_{hm} + C_{ps} + C_{pm} + C_{\text{PV}} \quad (13)$$

where:

$$C_{hm} = \frac{1}{365} \cdot k_{bo.f} \cdot P_r^b + k_{bo.v} \cdot P_r^b \cdot T_{bh} \quad (14)$$

$$C_{ps} = 0.75 \cdot \left(P_{\text{tot.T}} + P_{\text{tot.D}} \right) \cdot T_p \quad (15)$$

$$C_{pm} = \kappa_1 \cdot C_{pi} + \frac{1}{365} \cdot \lambda \cdot \left(C_{ps} + C_{lt} \cdot T_{\text{MTTR}} \right) \quad (16)$$

3.2.3 Replacement cost

The battery replacement cost C_{Rep} is represented as (17).

$$C_{\text{Rep}} = \frac{1}{365} \cdot CRF \cdot \sum_{k=1}^{N_R} \left(k_{br} \cdot E_r^b \right) \quad (17)$$

$$N_R = \left\lceil \frac{T_{\text{proj}}}{T_b} \right\rceil - 1 \quad (18)$$

where $\lceil \ \rceil$ represents the round up operator.

3.2.4 Disposal and recovery (D&R) cost

The D&R cost of co-phase TPSS $C_{\text{D\&R}}$ is the recoverable value that battery has not reached the end of its service life and the remaining material after PFC is disassembled, as (19).

$$C_{\text{D\&R}} = \kappa_2 \cdot \frac{\left(N_R + 1 \right) \cdot T_b - T_{\text{proj}}}{365 \cdot T_b} \cdot k_{bp} \cdot P_r^b + \kappa_3 \cdot C_{pi} \quad (19)$$

3.3. The capacity programming model based on the LCC of co-phase TPSS

Taking the minimum LCC of co-phase TPSS as the objective function, and taking P_r^{b}, E_r^{b}, P_r^{u}, E_r^{u} and S_{PFC} as decision variables, a capacity programming model based on LCC is established to acquire the optimal configuration capacity of HESS-PFC, and the most economical planning scheme. The capacity programming model is as follows in (20). Note that all costs are calculated on a daily basis.

$$\min C_{\text{LCC}} = \left(C_{\text{Inv}} \cdot CRF + C_{\text{O\&M}} + C_{\text{Rep}} - C_{\text{D\&R}} \cdot SFF \right) + C_e$$
$$s.t. \begin{cases} S_{\text{PFC.min}} \le S_{\text{PFC}} \le S_{\text{PFC.max}} & \\ P_{\min}^j \le P_r^j \le P_{\max}^j & j = bat, uc \\ E_{\min}^j \le E_r^j \le E_{\max}^j & \end{cases} \quad (20)$$

where: C_{Inv}~$C_{\text{D\&R}}$ and C_{e} are respectively described in detail in III-3.2 and IV-4.2, corresponding to formulas (10)-(19) and (21)-(26), then it is not necessary to list here again.

$$CRF = \frac{r(1+r)^{T_{\text{proj}}}}{(1+r)^{T_{\text{proj}}} - 1}, \quad SFF = \frac{r}{(1+r)^{T_{\text{proj}}} - 1}$$

4. Lower layer: Scheduling optimization model

4.1. PV output power uncertainty model

PV power generation system is affected by solar intensity, season and other factors. It is necessary for the uncertain behavior of PV power generation to be a model. Therefore, the scenario reduction method is employed to cope with the uncertainty of PV power in this paper [21]. taking the annual solar irradiance data of a certain place as an example [22], the original 365 solar irradiance scenarios are reduced to 6 scenarios, as shown in Fig. 5. It not only retains the characteristics of the original light intensity scene to the greatest extent but also greatly reduces the computational complexity.

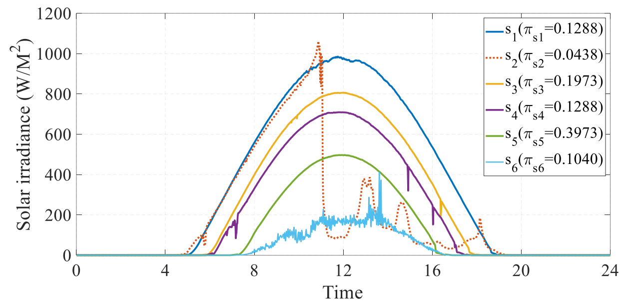

Fig. 5. Typical solar irradiance scenarios and probabilities generated by scene reduction techniques.

4.2. Optimized scheduling model of co-phase with PV and HESS

The objective function of the lower-layer model is the sum of short-term operating cost for electrified railway operators, including energy consumption cost (C_{ECC}), demand electricity cost (C_{DC}) and penalty cost (C_{PC}), taking $P_{t,s}^{\alpha}, P_{t,s}^{\beta}, Q_{t,s}^{\beta}, E_{t,s}^{b}, T_{bh}$ as decision variables. The optimized scheduling model is as follows in (21).

$$\begin{aligned} &\min C_e = C_{\text{ECC}} + C_{\text{CD}} + C_{\text{PC}} \\ &s.t. \ (39-54) \end{aligned} \quad (21)$$

where:

$$C_{\text{ECC}} = \sum_s \sum_{t=1}^{N_{\text{T}}} \pi_s \cdot \rho_{t,s}^{\text{grid}} \cdot P_{t.s}^{\text{grid}} \cdot \Delta t \quad (22)$$

$$C_{\text{DC}} = \sum_s \sum_{t=1}^{N_{\text{T}}} \pi_s \cdot \rho_{t,s}^{\text{dem}} \cdot \max(P_{t,s}^{\text{dem}}) \quad (23)$$

$$P_t^{\text{dem}} = \sum_s \sum_t^{t+14} \pi_s \cdot P_{t,s}^{\text{grid}} / 15 \qquad \forall t = 1, 2, ..., N_{\text{T}} - 14 \quad (24)$$

$$C_{\text{PC}} = \sum_s \sum_{t=1}^{N_{\text{T}}} \pi_s \cdot \rho_{t,s}^{\text{fed}} \cdot P_{t,s}^{\text{fed}} \cdot \Delta t \quad (25)$$

$$C_{\text{PV}} = \sum_s \sum_{t=1}^{N_{\text{T}}} \pi_s \cdot \rho_{t,s}^{\text{PV}} \cdot P_{t,s}^{\text{PV}} \cdot \Delta t \quad (26)$$

C_{ECC} represents the energy consumption of TPSS supplied by power grid in (22). In (23), C_{DC} is determined by the maximum value of averaged active power through traction transformer in 15 consecutive minutes time intervals during a month (or a day, assuming that daily operation of co-phase TPSS is repeated every day in this paper, a cycle is one day). C_{PC} denotes the penalty bill for the energy fed back to the power grid from TPSS in (25).

4.3. Constraints

4.3.1 Power flow balance constraints

Eq. (27) indicates that the active power transmission between TPSS and power grid takes α-phase converters and single-phase traction transformer (TT) as channels. Eq. (28) denotes the power balance in the direct-current link of PFC. Eq. (29) states the active power balances among TT, PFC and traction load. Eq. (30) assumes that the reactive power of the traction load is completely compensated by the β-phase converter in this paper. Eq. (31) and (32) imply that the power transfer direction between the co-phase TPSS and the power grid is specified by the binary variable v_t^{grid} so that the power purchased from the power grid and the energy fed back to the power grid cannot coexist simultaneously.

$$P_{t,s}^{\text{grid}} - P_{t,s}^{\text{fed}} = P_{t,s}^{\alpha} + P_{t,s}^{\text{T}} \tag{27}$$

$$P_{t,s}^{\alpha} + P_{t,s}^{\text{PV}} + P_{t,s}^{\text{b,dis}} + P_{t,s}^{\text{u,dis}} = P_{t,s}^{\beta} + P_{t,s}^{\text{b,ch}} + P_{t,s}^{\text{u,ch}} \tag{28}$$

$$P_{t,s}^{\beta} + P_{t,s}^{T} = P_{t,s}^{\text{TL}} - P_{t,s}^{\text{RBE}} \tag{29}$$

$$Q_{t,s}^{\beta} = Q_{t,s}^{\text{TL}} - Q_{t,s}^{\text{RBE}} \tag{30}$$

$$0 \le P_{t,s}^{\text{grid}} \le v_{t,s}^{\text{grid}} \cdot P_{t,s}^{\text{grid.max}} \tag{31}$$

$$0 \le P_{t,s}^{\text{fed}} \le (1 - v_{t,s}^{\text{grid}}) \cdot P_{t,s}^{\text{grid.max}} \tag{32}$$

4.3.2 HESS constraints

Eq. (33) indicates that the stored energy of battery and UC during the time interval t is limited to the presupposed upper and lower bounds determined by the parameters of selected energy storage device to avoid additional lifetime loss resulting from overcharge and over-discharge, as well as into account charge and discharge efficiency and self-discharge rate. To facilitate the daily scheduling of co-phase TPSS, the stored energy of battery and UC at initial time should be equal to that at the last time respectively, presented by (34). Eq. (35) represents the charging and discharging process of the battery and UC determined by binary variables v_t^j, when equal to 1, it means the battery and UC are in discharging state, otherwise, it is in charging state. Eq. (36) is used to calculate the number of operating hours per day for battery.

$$SOC_{\min}^{j} E_r^{j} \le (1-\varepsilon_j) E_{t-1,s}^{j} + \eta_{\text{ch}}^{j} P_{t-1,s}^{j.\text{ch}} \Delta t - \frac{P_{t-1,s}^{j.\text{dis}} \Delta t}{\eta_{\text{dis}}^{j}} \le SOC_{\max}^{j} E_r^{j} \tag{33}$$

$$E_{t=1,s}^{j} = E_{t=N_T,s}^{j} = SOC_{t=0}^{j} \cdot E_r^{j} \tag{34}$$

$$0 \le P_{t,s}^{j,\text{dis}} \le v_{t,s}^{j} \cdot P_r^{j}, 0 \le P_{t,s}^{j,\text{ch}} \le (1 - v_{t,s}^{j}) \cdot P_r^{j} \tag{35}$$

$$T_{bh} = \sum_{s}\sum_{t} \pi_s \cdot v_{t,s}^{b} \cdot \Delta t \tag{36}$$

4.3.3 PV constraints

In the optimal scheduling of co-phase TPSS, PV output is non-negative and constrained by the maximum predicted value ($P_t^{\text{PV.max}}$). PV converter can control output in real time during operation, so real output of PV constraint is revised as (37).

$$0 \le P_{t,s}^{\text{PV}} \le P_{t,s}^{\text{PV.max}} \tag{37}$$

4.3.4 Three-phase voltage unbalance constraints

The negative sequence problem measured by three-phase voltage unbalance is the most important power quality problem of electrified high-speed and heavy-haul railway. The three-phase voltage unbalance u_ε is described by the ratio of the negative sequence power S^- to short circuit capacity S_d of power system at the common connection point, and meet the limitation required by the power quality standard 2% [23].

$$u_\varepsilon = \frac{S^-}{S_d} \times 100\% = \frac{\sqrt{3} \times U_S \times |\boldsymbol{I}_t^{(-)}|}{S_d} \times 100\% \le u_{\varepsilon.\max} \tag{38}$$

According to [9], the negative sequence current in grid side can be deduced as.

$$\begin{aligned} \boldsymbol{I}_t^{(-)} &= \frac{1-a}{3N_1} \boldsymbol{I}_{\text{T}} + \frac{a^2}{3N_2} \boldsymbol{I}_{\alpha} \\ &= \underbrace{\frac{1}{\sqrt{3}N_1} e^{-j(60^\circ + \varphi_{\text{T}})} \cdot \frac{P_{t,s}^{\text{T}}}{U^{\text{T}}}}_{\text{Part I}} + \underbrace{\frac{1}{3N_2} e^{j(120^\circ - \varphi_{\alpha})} \cdot \frac{P_{t,s}^{\alpha}}{U^{\alpha}}}_{\text{Part II}} \end{aligned} \tag{39}$$

where $a = e^{j120}$.

The negative sequence current can be split into two parts, one is caused by active power of TT and the other by active power of α-phase converter. Due to these two parts do not participate in the transmission of reactive power between the power grid and TPSS in this paper, $\varphi_{\text{T}} = \varphi_\alpha = 0$. Accordingly, the amplitude of negative sequence current is presented as

$$\left| \boldsymbol{I}_t^{(-)} \right| = \left| \frac{P_{t,s}^{\text{T}}}{\sqrt{3} U^{\text{T}} N_1} - \frac{P_{t,s}^{\alpha}}{3 U^{\alpha} N_2} \right| \tag{40}$$

4.3.5 PFC operating boundary constraints

Active power and reactive power flowing through α and β-phase converters are constrained by their rated capacity, and are denoted in (41) and (42).

$$\sqrt{\left(P_{t,s}^{\alpha}\right)^2 + \left(Q_{t,s}^{\alpha}\right)^2} \le S_\alpha \tag{41}$$

$$\sqrt{\left(P_{t,s}^{\beta}\right)^2 + \left(Q_{t,s}^{\beta}\right)^2} \le S_\beta \tag{42}$$

Assuming that α-phase converter not participate in the transmission of reactive power in this paper. Therefore, the constraint (41) is equivalent to the following (43).

$$-S_\alpha \le P_{t,s}^{\alpha} \le S_\alpha \tag{43}$$

Particularly, $P_{t,s}^{\alpha}, P_{t,s}^{\beta}, Q_{t,s}^{\beta}$ optimized by the lower layer are used as the input variables of the upper layer to evaluate the PFC reliability.

5. Solution Methodology: Whale optimization algorithm with GUROBI solver embedded

5.1. Overview of whale optimization algorithm

5.1.1 Bubble-net attacking (Exploitation phase)

Humpback whales achieve the purpose of local optimization by surrounding their prey and spirally updating their positions. The behavior of whales surrounding prey is described in (44)-(48).

$$\boldsymbol{X}(t+1) = \boldsymbol{X}^*(t) - \boldsymbol{A} \cdot \boldsymbol{D} \tag{44}$$

$$\boldsymbol{D} = \left| \boldsymbol{C}\boldsymbol{X}^*(t) - \boldsymbol{X}(t) \right| \tag{45}$$

$$\boldsymbol{A} = 2\boldsymbol{a}\cdot\boldsymbol{r}_1 - \boldsymbol{a} \quad (46)$$

$$\boldsymbol{a} = 2 - 2t / t_{\max} \quad (47)$$

$$\boldsymbol{C} = 2\cdot\boldsymbol{r}_2 \quad (48)$$

where t and $t_{\max}$ indicate the current iteration number and the maximum iterations number. $\boldsymbol{X}^*$ and $\boldsymbol{X}$ represent the global optimal whale position vector and the current whale position vector, respectively. $\boldsymbol{A}$ and $\boldsymbol{C}$ are the coefficient vector. $\boldsymbol{r}_1$ and $\boldsymbol{r}_2$ are random vector within [0, 1].

The mathematical model of humpback whales swimming to prey in a spiral path is shown in (57).

$$\boldsymbol{X}\left(t+1\right) = \boldsymbol{D}'\cdot e^{bl}\cdot\cos(2\pi l) + \boldsymbol{X}^*\left(t\right) \quad (49)$$

$$\boldsymbol{D}' = \left|\boldsymbol{X}^*(t) - \boldsymbol{X}(t)\right| \quad (50)$$

where b defines the shape constant of the logarithmic spiral, l is a random number within [-1,1].

However, humpback whales have special behavior that not only swims around their prey in a shrinking circle but also swims along simultaneously a spiral path. p is introduced to determine the probability of two predation methods and is a random number within [0,1]. The updated position of whale is as follows (51).

$$\boldsymbol{X}(t+1) = \begin{cases} \boldsymbol{X}^*(t) - \boldsymbol{A}\cdot\boldsymbol{D} & p < 0.5 \\ \boldsymbol{D}'\cdot e^{bl}\cdot\cos(2\pi l) + \boldsymbol{X}^*(t) & p \geq 0.5 \end{cases} \quad (51)$$

5.1.2 Random search (Exploration phase)

Humpback whales will randomly search based on coefficient vector $\boldsymbol{A}$ ($|\boldsymbol{A}|>1$), as shown in (52).

$$\boldsymbol{X}(t+1) = \boldsymbol{X}_{\text{rand}} - \boldsymbol{A}\cdot\boldsymbol{D}' \quad (52)$$

$$\boldsymbol{D}' = \left|\boldsymbol{C}\cdot\boldsymbol{X}_{\text{rand}} - \boldsymbol{X}\right| \quad (53)$$

where $\boldsymbol{X}_{\text{rand}}$ indicates a randomly selected whale position vector.

5.2. Piecewise linearization

For the purpose of reducing the complexity of the model and improving the solution speed, it is necessary to linearize the nonlinear formulas such as the electricity demand electricity cost, PFC apparent power, and three-phase voltage unbalance constraints in the lower layer model by linearization means. Therefore, a mixed integer linear programming problem is formulated and GUROBI commercial solver is adopted to solve this problem.

5.2.1 Linearization of demand electricity cost

In order to reduce the computational burden, the maximum function in (23) is linearized by introducing an auxiliary variable P_t^{peak}, as shown in (54) and (55).

$$\max(P_{t,s}^{\text{dem}}) = P_{t,s}^{\text{peak}} \quad (54)$$

$$P_{t,s}^{\text{dem}} \leq P_{t,s}^{\text{peak}} \quad \forall t = 1,2,\ldots,N_T - 14 \quad (55)$$

5.2.2 Three-phase voltage unbalance constrained linearization

Linearize the above Eq. (40) by introducing auxiliary non-negative variables p_t^{T} and p_t^{α}, binary variables v_t^{p} based on the big-M method to improve calculation speed.

$$\left|\boldsymbol{I}_t^{(-)}\right| = \left|\frac{P_{t,s}^{\text{T}}}{\sqrt{3}U^{\text{T}}N_1} - \frac{P_{t,s}^{\alpha}}{3U^{\alpha}N_2}\right| = p_{t,s}^{\text{T}} + p_{t,s}^{\alpha} \leq \frac{u_{\varepsilon.\max}S_d}{\sqrt{3}U_S} \quad (56)$$

$$\frac{P_{t,s}^{\text{T}}}{\sqrt{3}U^{\text{T}}N_1} - \frac{P_{t,s}^{\alpha}}{3U^{\alpha}N_2} = p_{t,s}^{\text{T}} - p_{t,s}^{\alpha} \quad (57)$$

$$0 \leq p_{t,s}^{\text{T}} \leq v_{t,s}^{p}M \;\;,\;\; 0 \leq p_{t,s}^{\alpha} \leq \left(1 - v_{t,s}^{p}\right)M \quad (58)$$

5.2.3 PFC apparent power linearization

In (42), the essence of the PFC capacity constraint is a PQ circular constraint composed of active power and reactive power. The circumscribed square of multiple circles method [24] is used to achieve an approximate expression of the circle in this paper. Under the premise of ensuring accuracy, this paper chooses three circumscribed square constraints to linearize the PFC capacity, and the specific expression is denoted as (59).

$$\begin{cases} -S_\beta \leq P_{t,s}^{\beta} \leq S_\beta \\ -S_\beta \leq Q_{t,s}^{\beta} \leq S_\beta \\ -2S_\beta \leq \sqrt{3}P_{t,s}^{\beta} + Q_{t,s}^{\beta} \leq 2S_\beta \\ -2S_\beta \leq \sqrt{3}P_{t,s}^{\beta} - Q_{t,s}^{\beta} \leq 2S_\beta \\ -2\sqrt{3}S_\beta \leq \sqrt{3}P_{t,s}^{\beta} + 3Q_{t,s}^{\beta} \leq 2\sqrt{3}S_\beta \\ -2\sqrt{3}S_\beta \leq \sqrt{3}P_{t,s}^{\beta} - 3Q_{t,s}^{\beta} \leq 2\sqrt{3}S_\beta \end{cases} \quad (59)$$

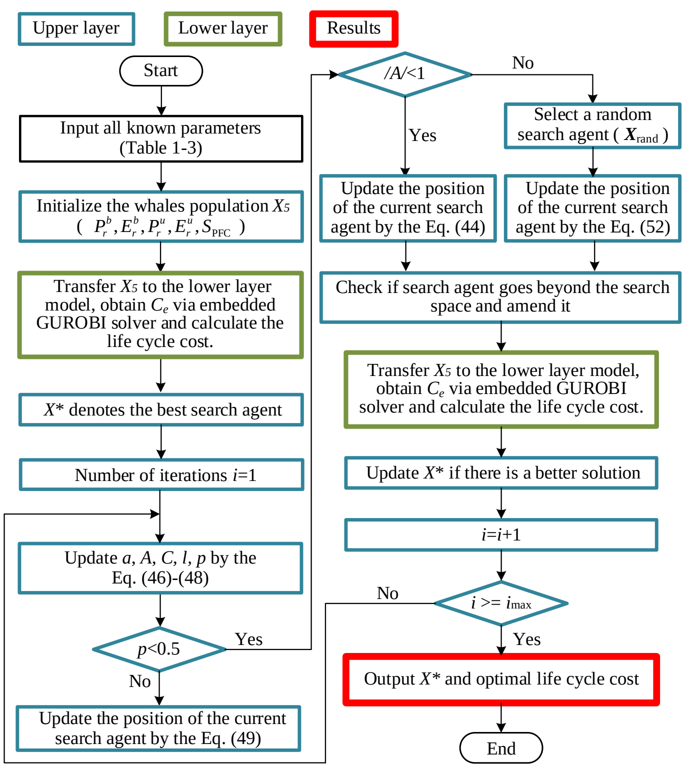

Fig. 6. Block diagram of WOA with GUROBI solver embedded.

5.3 Application of WOA with GUROBI solver embedded

In the upper layer, the linearization of PFC and battery lifetime calculation is hard to be realized by the linear programming method. Therefore, WOA [25] is adopted to plan the capacity of HESS-PFC. In the lower layer, it is formulated as MILP model, which is solved to obtain HESS operation strategy and PFC compensation powers by GUROBI solver.

WOA with GUROBI solver embedded approach is adopted to deal with this bi-hierarchy problem. In WOA, given the number of particles N, the position of each search agent can be expressed as a five-dimensional vector x_i = [x_{i1}, x_{i2}, x_{i3}, x_{i4}, x_{i5}], which represents the decision variables P_r^{b}, E_r^{b}, P_r^{u}, E_r^{u}, S_{PFC} in the upper model, respectively. The block diagram and overall pseudo code of applying WOA with GUROBI solver embedded to settle HESS-PFC capacity and diurnal dispatch problems are illustrated in Fig. 6 and Algorithm 1.

Algorithm1. WOA with GUROBI solver embedded

```
Input: Traction load, PV output and price. (Table 2-4)
Set the number of search agents (N), max number of iterations t_max
Initialization: Humpback whale population X_i (i=1, 2, …, n)
Transfer X_i to the lower layer model, obtain C_e via embedded GUROBI
solver and calculate life cycle cost
X* denotes the best search agent
while (t< t_max)
  for each search agent
  Update a, A, C, l and p by Eq. (46)-(48)
    if1 (p<0.5)        % Shrinking and enveloping mechanism
      if2 (/A/<1)      % Exploitation phase
        Update the position of the current search agent by Eq. (44)
      else if2 (/A/>=1)     % Exploration phase
        Select a random search agent (X_rand)
        Update the position of the current search agent by Eq. (52)
      end if2
    else if (p>=0.5)       % Spiral update position
        Update the position of the current search agent by Eq. (49)
    end if1
  end for
Check if any search agent goes beyond the search space and amend it
Transfer X_i to the lower layer model, obtain C_e via embedded GUROBI
solver and calculate life cycle cost
Update X* if there is a better solution
t=t+1
end while
Output X* and optimal life cycle cost
```

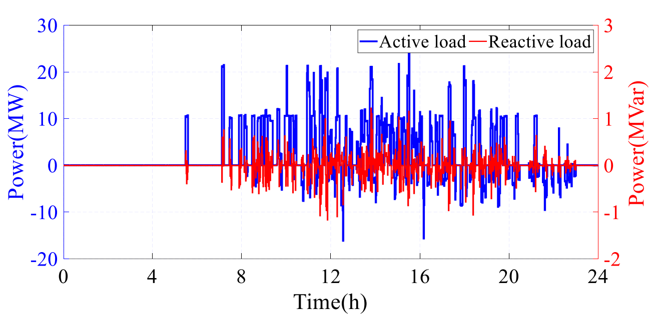

Fig. 7. Traction load data.

6. Case studies

6.1 Input parameters

Take a typical TPSS of a high-speed rail line in northwest China as an example, PV output power is presented in Fig. 5, and the data of traction load are outlined in Fig. 7. Traction load has the characteristics of shock and random fluctuation. Due to the particularity of the power supply system and the asymmetry of the traction load, it will cause three-phase unbalance on the grid side. Related parameters of system unit cost, electricity prices and co-phase TPSS are listed in Table 2-4 [8, 13, 17-20, 26-28]. It is assumed that the upper and lower bounds of decision variables of the upper layer model are P_r^{b} ∈[1, 4] MW, E_r^{b} ∈[5, 15] MWh, P_r^{u} ∈[10, 20] MW and E_r^{u} ∈ [0.1, 0.5] MWh, S_{PFC} ∈[5, 12] MVA. The optimization process in this manuscript is implemented on a computer with Intel Core i5-1135G7 CPU at 2.4 GHz and 16 GB RAM. The optimization problem in the upper and lower layer is solved using the YALMIP toolbox (version 20190425) [29] and GUROBI solver (version 9.5.1) [30] integrated with the software environment of MATLAB (version 2018a).

Table 2
Cost parameters

Components	Parameters	Battery	UC
HESS	k_{bp} / k_{up} CNY/kW	2138	1680
	k_{be} / k_{ue} CNY/kWh	3240	61800
	k_{br} CNY/kWh	1292	/
	k_{bop} CNY/kW	423	423
	$k_{bo.f}$ CNY/kW/year	25.5	/
	$k_{bo.v}$ CNY/kW/h	2.78	/
	$\eta_{\mathrm{ch}}^{\mathrm{b/u}}$ / $\eta_{\mathrm{dis}}^{\mathrm{b/u}}$	0.8/0.8	0.95/0.95
	[$SOC_{\mathrm{min}}^{\mathrm{b/u}}$, $SOC_{\mathrm{max}}^{\mathrm{b/u}}$]	[0.2,0.8]	[0.05,0.95]
	$SOC_{\mathrm{t=0}}^{\mathrm{b/u}}$	0.5	0.5
	$\varepsilon_{\mathrm{b/u}}$/day	0.1%	/
	κ_2	0.7	0.7
PFC	k_{PFC} CNY/kW	500	
	κ_1	5%	
	κ_3	15%	
	T_p /h	8760	
	C_{lt} CNY/kW/year	1400	
PV	k_{PV} CNY/kW	0.1	

Table 3
Parameters of electricity price

Type of electricity price			Period	Price
ρ_t^{grid} / ρ_t^{fed}	TOU	Valley(¥/kWh)	0-6h, 22-0h	0.370
		Peak(¥/kWh)	8-11h, 18-21h	1.252
		Intermediate(¥/kWh)	7-8h, 12-17h	0.782
	Fixed	¥/kWh	0-0^{+1}h	0.782
ρ_t^{dem}		¥/kWh/Mon	0-0^{+1}h	42

Table 4
Technical parameters of co-phase TPSS

Parameters	Value
Rated line voltage in three-phase side U_S	110 kV
Grid short-circuit capacity S_d	750 MVA
Three-phase voltage unbalance limit $u_{\varepsilon.\mathrm{limit}}$	2%
TT output voltage U_{T}	27.5kV
α phase voltage U_α	10 kV
β phase voltage U_β	10 kV
Ratio of TT N_1	4
Ratio of HMT N_2	$11/\sqrt{3}$

Table 5
The details on the case studies

Case	Systems	PV	HESS		Electricity Schemes	Variables Number
			Battery	UC		
Case1	TPSS	-	-	-	TOU	0
Case2	CTPSS	-	√	-	TOU	3
Case3	CTPSS	-	√	√	TOU	5
Case4	CTPSS	√	√	√	Fixed	5
Case5	CTPSS	√	√	√	TOU	5

6.2 Cost results analysis in different cases

Five separate case studies are performed to show the feasibility of the proposed capacity programming model, taking into account the existence of PV, HESS composed of battery and UC, as well as electricity schemes. Table 5 contains the details of the case studies.

Case 1: The conventional TPSS without PV and HESS [7], adopts time-of-use (TOU) tariff, as a base reference;

Case 2: A co-phase TPSS with battery, adopts TOU tariff;

Case 3: The co-phase TPSS with HESS consisting of battery and UC, adopts TOU tariff;

Case 4: A co-phase TPSS with PV and HESS shown in Fig. 1, adopts Fixed tariff;

Case 5: The co-phase TPSS with PV and HESS, adopts TOU tariff.

The LCC results of co-phase TPSS are listed in Table 6. Case 1 is to serve as the basic control group, which is no PV and HESS accessed. In Case-1, short-term operating cost is 98967 CNY and equals to LCC of co-phase TPSS. The main difference between Case-2 and Case-3 is the type of energy storage device. The former uses only the battery, while the latter adopts HESS consisting of battery and UC. The short-term operating cost C_e and C_{LCC} of Case-2 are higher than those of Case-3, and even higher than Case-1, because the replacement cost of the battery is taken into account. Compared with Case-1, the optimal results obtained show that the LCC of Case-2 is increased by 4.78% and Case-3 is reduced by 7.80%. It can be illustrated that HESS has more advantages than a single battery in terms of traction load peak-shaving and valley-filling and RBE utilization. It can be further confirmed that the peak load power of co-phase TPSS has been shaved and RBE has been largely recycled between 12:00 A.M and 14:00 A.M in Fig. 8(a) and Fig. 8(b), which contributes to reducing C_{ECC}, C_{DC} and C_{PC}.

Table 6
The LCC in different cases

Case/CNY	Case-1	Case-2	Case-3	Case-4	Case-5
C_{ECC}	81837	59436	55739	37873	45087
C_{DC}	17130	13004	11655	10113	10538
C_{PC}	14760	4116	1137	987	1819
C_e	98967	76556	68531	48973	57444
C	/	27143	22721	24709	18501
C_{LCC}	98967	103699	91252	73682	75945
R_e%	/	22.64%	30.75%	50.51%	41.96%
R_t%	/	-4.78%	7.80%	25.55%	23.26%

R_e%——Short-term operating cost C_e reduction rate (Compare with Case-1);
R_t%——LCC C_{LCC} reduction rate (Compare with Case-1).

The access of PV is to improve the utilization of renewable energy. Case-5 is connected to PV based on the scenario of Case-3, the reduction rate of the LCC is 23.26%. However, penalty charge C_{PC} is slightly higher than Case-3, mainly because the PV is like a source that only provides energy rather than absorb energy. In other words, PV accessed can reduce C_{ECC} and C_{DC}, as shown in Fig. 8(c). Case-4 is distinct from Case-5 in terms of electricity price schemes. The short-term operating cost of co-phase TPSS in Case-5 is 57444 CNY, which is much higher than cost 48973 CNY in Case-4. It is mainly because the peak period of traction load corresponds to peak or intermediate electricity price. The valley electricity price coincides with the railway skylight period when the load is almost zero, which causes enormous differences in electricity.

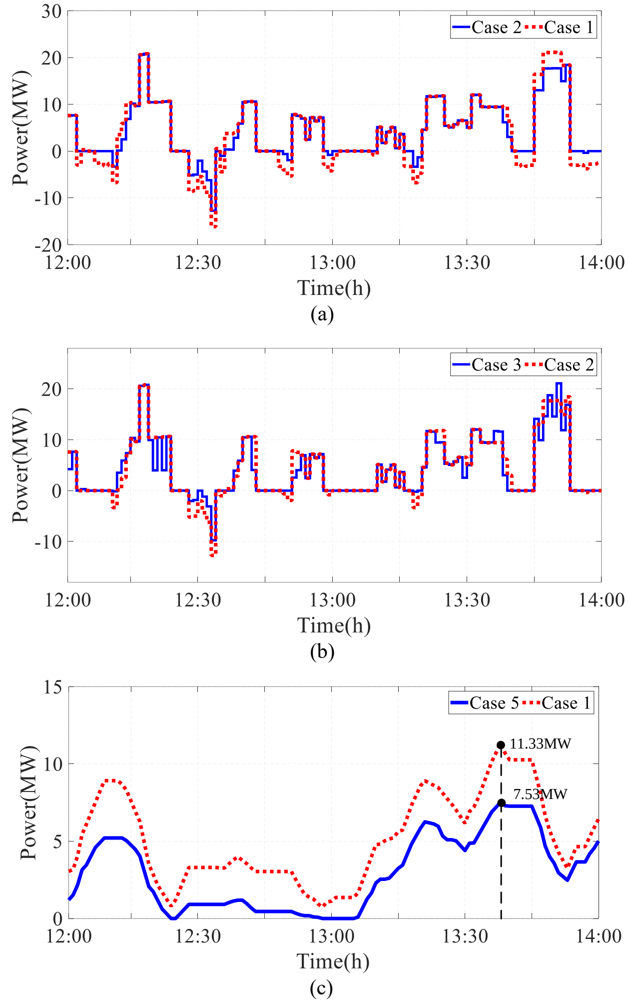

Fig. 8. (a) Power of utility grid in Case-1 and Case-2; (b) Power of utility grid in Case-3 and Case-2; (c) Demand power in Case-1 and Case-5

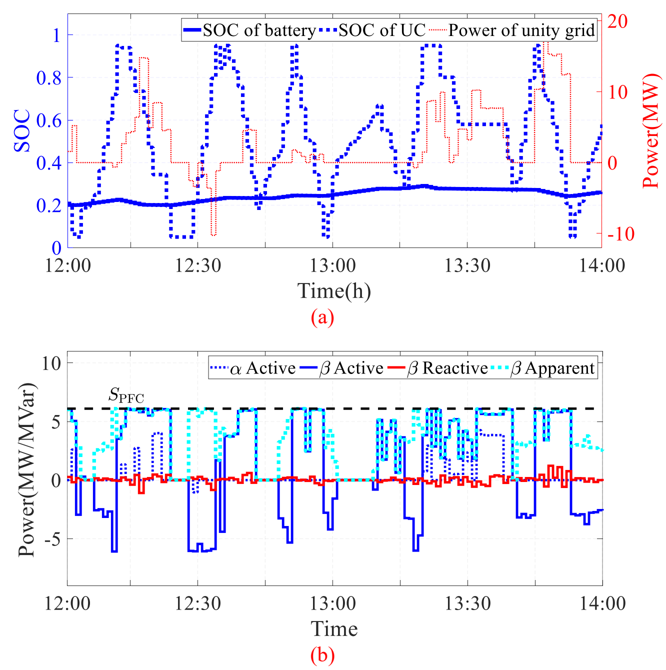

Fig. 9. (a) SOC of battery and UC; (b) Active power of α-phase converter and active, reactive and apparent power of β-phase converter in Case-5.

The charge and discharge number of UC is much higher than that of battery in Fig. 9(a). UC is mainly responsible for high-frequency shock load response due to its high cycle lifetime and rapid response, while the battery is mainly responsible for responding to long-term energy demand due to its high energy density and short cycle lifetime. Fig. 9(b) shows power flow of β-phase converter. Due to the charge and discharge of HESS, β-phase converter absorbs power from α-phase converter, HESS, PV or RBE, so it can be observed that active power of β-phase converter is significantly greater than that of α-phase converter. In addition, the apparent power S_β of β-phase converter is always not greater than its rated capacity S_{PFC} (optimized variable in this paper), which proves the effectiveness of the PFC capacity constraint linearization.

Table 7
Optimal capacity and lifetime results in different cases

Case	Case-2	Case-3	Case-4	Case-5
P_r^{b} /MW	3.4	2.3	3.5	1.2
E_r^{b}/MWh	6.5	6.2	6.6	5.5
P_r^{u}/MW	/	11.6	13.5	10.1
E_r^{u}/MWh	/	0.43	0.4	0.48
S_{PFC}/MVA	13.4	13.2	12.6	12.2
T_b/year	1.47	2.35	2.71	2.93
T_{MTTF} /year	13.63	14.99	18.35	21.56

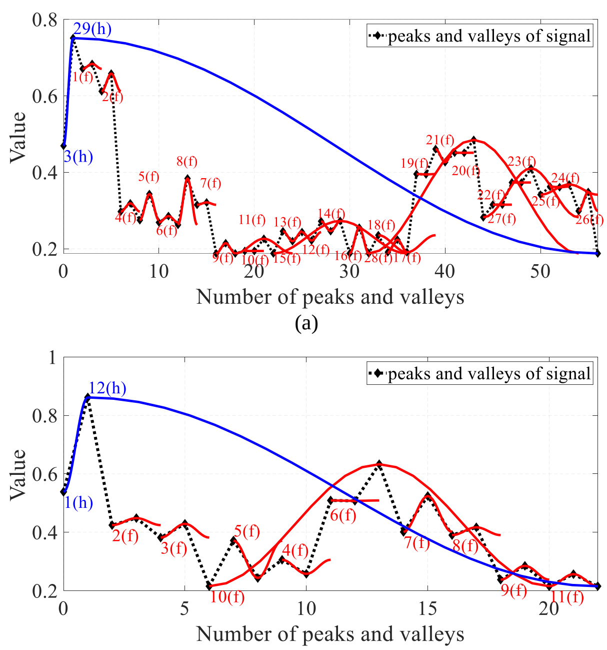

h——Half cycles; f——Full cycles.

Fig. 10. (a) and (b) Cycles identification of battery SOC in Case-2 and Case-3, respectively.

6.3 Lifetime of battery and PFC

The optimal capacity and lifetime results of co-phase TPSS under different cases are shown in Table 7. In Fig.10(a), the battery contains 27 full cycles and 2 half cycles in Case-2. By contrast, in Fig. 10(b), the battery contains 10 full cycles and 2 half cycles in Case-3, resulting in a significant of battery lifetime. The results are consistent with T_b in Table 7. The charging and discharging number of the battery is more frequent in Case-2, resulting in a faster battery aging, so the combination of the battery and UC is beneficial to prolong the battery lifetime.

Fig. 11 shows the PFC lifetime T_{MTTF} and IGBT modules junction temperature (T_{j} and ΔT_{j}) results on the traction side under different cases. In the comparison between Case-2 and Case-3, it is illustrated that HESS combining the advantages of battery and UC is superior to a single battery in PFC lifetime improvement. Furthermore, PV connected also can improve PFC lifetime to a certain extent. The PFC lifetime T_{MTTF} in Case-5 is larger than in Case-4. It means that the electricity price schemes affect the power flow distribution of co-phase TPSS, and then affect the PFC junction temperature. To sum up the above, adopting the proposed bi-hierarchy capacity programming strategy in this paper can decrease the junction temperature fluctuation and average junction temperature, thereby the PFC lifetime is prolonged to 21.56 years compared with Case-2 to Case-4.

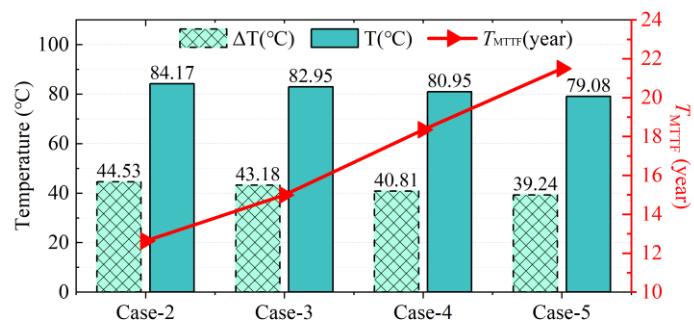

Fig. 11. Comparison of PFC lifetime T_{MTTF} and junction temperature of IGBTs in the traction side under different cases.

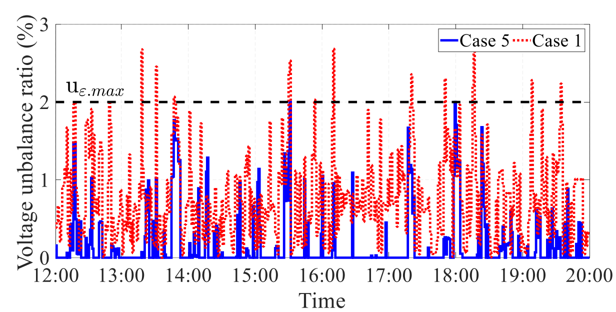

Fig. 12. Comparison of three-phase voltage unbalance in Case-5 and Case-1.

6.4 The effect of power quality control

For three-phase voltage unbalance caused by asymmetric traction load, the three-phase voltage unbalance constraint is taken into account in the optimization model of co-phase TPSS, the three-phase voltage unbalance limit is set to 2% in accordance with the IEC/TR 61000-3-13 standard. It can be seen from Fig. 12 that compared with the voltage unbalance of the traction substation in Case-1 that only uses TT, by reasonably distributing the power flow distribution of TT and PFC, the voltage unbalance in Case-5 is a large degree of reduction and bound by the standard. On the contrary, the three-phase voltage unbalance in Case-1 exists exceeding the IEC standard, and the maximum value is 2.79%.

6.5 The impact of initial SOC on short-term operating cost

Take Case-5 as an example, Fig. 13 shows the comparison result of short-term operating cost considering different initial SOC. A series of initial SOC values of 0.2, 0.3, 0.4, 0.5, 0.6, 0.7 and 0.8 are analyzed. It can be seen from Fig. 14 that a maximum short-term operating cost reduction of 46.65% compared with Case-1 is achieved with initial SOC of 0.5. If the initial SOC of HESS continues to increase, the effect of short-term operating cost reduction will be saturated.

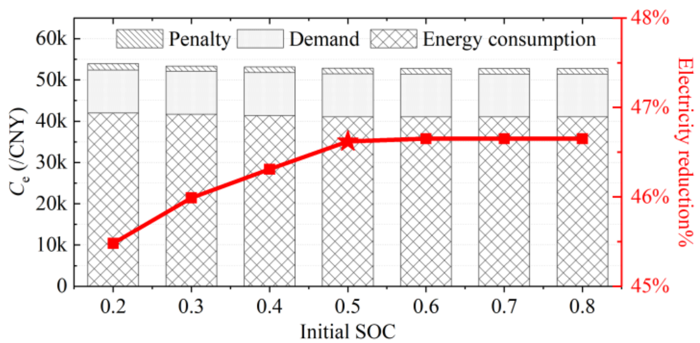

Fig. 13. Sensitivity analysis on the impact of initial SoC on electricity reduction.

Table 8
Comparison results of different optimization strategies

	Case 1	R_1	R_2	R_3	This paper
C_{LCC}/CNY	98967	90051	2364	91537	75945
C_e/CNY	98967	60441	/	65754	57444
C_{HESS}/CNY	/	28232	/	25783	16027
C_{PV}/CNY	/	1378	/	/	1289
C_{PFC}/CNY	/	/	2364	/	1184
T_b/year	/	1.84	/	1.81	2.93↑
T_{MTTF} /year	/	/	7.80	/	21.56↑
R_{LCC}%	/	9.01%	/	7.51%	23.26%↓

R_{PFC}%——Life cycle cost of PFC C_{PFC} reduction rate (Compare with R_2).

6.6 Comparison with existing literature

The comparison between reference [7, 18, 31] and this paper is presented in Table 8.

R_1: The conventional traction power supply system (TPSS) with HESS and PV, as shown in reference [7].

R_2: Only PFC, and PFC capacity is set 12MW in reference [18].

R_3: Co-phase TPSS with HESS, and PFC capacity is set 10MW in reference [31].

This paper: Co-phase TPSS with HESS and PV, and PFC capacity is optimized.

Case 1 is to serve as the basic control group, which is no PV and HESS accessed. R_1 is connected to HESS and PV on the basis of traditional TPSS, which reduces the short-term operating cost by 38.93% (from 98967 CNY to 60441 CNY) through the charging and discharging process of HESS, but inevitably increases the investment cost and O&M cost of HESS and PV, resulting in a final total cost reduction of only 9.01%. R_2 only considers the life cycle cost of PFC, and the PFC cost is calculated as 2364 CNY with the capacity set in reference [18]. The co-phase TPSS adopted in R_3 can effectively utilize the RBE and reduce the penalty cost caused by the energy feedback to the grid. However, the cost reduction rate is lower than that of reference [7]. This is because the HESS capacity is not reasonably optimized in reference [31]. Therefore, the bi-hierarchy capacity programming strategy adopted in this paper not only improves the RBE utilization to reduce short-term operating cost, but also reduces the life cycle cost of system by optimizing the capacity of HESS and PFC. It is seen from Table 8 that the cost reduction effect of this paper is better than that of the references [7, 18, 31].

In addition, an integrated lifetime evaluation model of HESS-PFC in this paper is used to assess the battery and PFC lifetime further. Compared with reference [7] and [18], the method proposed in this paper can prolong the battery lifetime to 2.93 years, which is the key to reduce the long-term investment cost of battery. The optimization process of PFC capacity between reference [7] and this paper is inconsistent. Reference [17] is an open-loop state, the enumeration method is used to determine the PFC capacity. By contrast, this paper forms a closed loop, an integrated lifetime evaluation model of HESS-PFC is constructed and a bi-hierarchy capacity programming strategy is adopted to simultaneously optimize PFC capacity and extend PFC lifetime for minimum life cycle cost. It is shown in Table 8 that the PFC lifetime can be extended from 7.80 years to 21.56 years, an extension of 63.82%, and a reduction of 49.91% in the PFC life cycle cost by optimizing the PFC capacity.

The convergence of solving methods for capacity programming is compared as shown in Fig. 14. Reference [7] adopts the gray wolf algorithm (GWO), and reference [18] uses the particle swarm algorithm (PSO). In this paper, the whale optimization algorithm (WOA) with embedded GUROBI solver is used. It can be seen from Fig. 14 that the WOA converges to 75.95k CNY in the eighth iteration, which is better than the other two algorithms. In addition, the best solution of WOA in the first generation is also obviously lower than that of the other two algorithms, which further proves that WOA has a strong superiority.

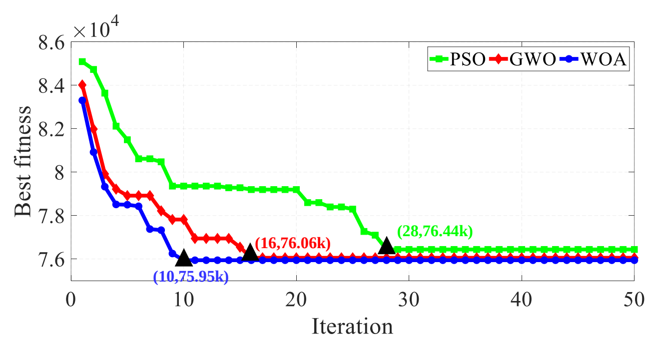

Fig. 14. Convergence curves of PSO, GWO and WOA

7. Conclusion

In this paper, a bi-hierarchy capacity programming model of co-phase TPSS with PV and HESS is proposed to optimize HESS-PFC capacity for minimum life cycle cost. Meanwhile, the proposed method can improve technical metrics, including three-phase voltage unbalance, and the battery and PFC lifetime, as well as remove neutral section. Furthermore, whale optimization algorithm with GUROBI solver embedded is employed to solve this model.

Case studies reveal that the life cycle cost and short-term operating cost of co-phase TPSS with PV and HESS in this paper can be reduced respectively by 23.26% and 41.96% compared with traditional co-phase TPSS. Meanwhile, three-phase voltage unbalance of co-phase TPSS is within the allowable range of the IEC standard (2%), which proves the effectiveness of co-phase TPSS to improve energy utilization and power quality. Besides, HESS has more advantages than a single battery in terms of traction load peak-shaving and valley-filling, RBE utilization improvement, and PFC lifetime improvement. Compared with existing literature, PFC lifetime is enhanced by 63.82% (from 7.80 years to 21.56 years) and battery lifetime is prolonged to 2.93 years. In addition, the whale optimization algorithm with GUROBI embedded has been proved to have a strong superiority.

Funding

This paper was supported by the National Natural Science Foundation of China under Grant 51877182.

CRediT Authorship Contribution Statement

Minwu Chen: Supervision, Conceptualization, Writing - review & editing. **Xin Gong**: Conceptualization, Methodology, Writing - original draft, Writing - review & editing. **Zongyou Liang**: Software, Visualization, Writing - original draft, Writing - review & editing. **Jinyu Zhao**: Methodology, Writing - original draft. **Zhongbei Tian**: Methodology, Visualization.

Conflict of interest

The authors declare that they have no known competing financial interests or personal relationships that could have appeared to influence the work reported in this paper.

References

[1] Serrano-Jiménez D, Lopez-Lopez A, Pecharroman R, Cucala A, Fernandez-Cardador A. Electrical railway power supply systems: Current situation and future trends. Int J Electr Power Energy Syst 2017;92:181-192.

[2] Chen J, Hu H, Ge Y, Wang K, He Z. Techno-economic model-based capacity design approach for railway power conditioner-based energy storage system. IEEE Trans Ind Electron 2022;69(5):4730-4741.

[3] Chen M, Cheng Z, Liu Y, Chen Y, Tian Z. Multitime-scale optimal dispatch of railway FTPSS based on model predictive control. IEEE Trans Transp Electrif 2020;6(2):808-820.

[4] Hernandez J, Sutil F. Electric vehicle charging stations feeded by renewable: PV and train regenerative braking. IEEE Lat Am Trans 2016;14(7):3262-3269.

[5] Hernandez J, Sutil F, Vidal P. Protection of a multiterminal DC compact node feeding electric vehicles on electric railway systems, secondary distribution networks, and PV systems. Turk J Electr Eng Comput Sci 2016;24(4):3123-3143.

[6] Novak H, Lesic V, Vasak M. Hierarchical model predictive control for coordinated electric railway traction system energy management. IEEE Trans Intell Transp Syst 2019;20(7):2715-2727.

[7] Liu Y, Chen M, Lu S, Chen Y, Li Q. Optimized sizing and scheduling of hybrid energy storage systems for high-speed railway traction substations. Energies 2018; 11(9):2199-2228.

[8] Mousavi Gazafrudi SM, Tabakhpour Langerudy A, Fuchs EF, Al-Haddad K. Power quality issues in railway electrification: A comprehensive perspective. IEEE Trans Ind Electron 2015;62(5):3081-3090.

[9] Chen M, Li Q, Roberts C, Hillmansen S, Tricoli P, Zhao N, et al. Modelling and performance analysis of advanced combined co-phase traction power supply system in electrified railway. IET Gener Transmiss Distrib 2016;10(4):906-916.

[10] Tian H, Chen M, Zhang D, Wang M. A dynamic adjustment method of switching frequency used to improve the operating reliability of co-phase power flow controller. Proc CSEE 2021;41(11):3923-3932.

[11] Zhou L, Wu J, Sun P, Du X. Junction temperature management of IGBT module in power electronic converters. Microelectron Reliab 2014;54(12): 2788-2795.

[12] Chen M, Zhang D, Wang M, Lv Y, Chen Y. A lifetime extension strategy to increase the reliability of PFC in co-phase TPSS. Int J Electr Power Energy Syst 2021;130.

[13] Zhang Y, Xu Y, Yang H, Dong Z, Zhang R. Optimal whole-life-cycle planning of battery energy storage for multi-functional services in power systems. IEEE Trans Sustain Energy 2020;11(4):2077-2086.

[14] Hernandez J, Gomez-Gonzalez M, Sanchez-Sutil F, Jurado F. Optimization of battery/supercapacitor-based photovoltaic household-prosumers providing self-consumption and frequency containment reserve as influenced by temporal data granularity. J Energy Storage 2021;36:102366.

[15] Gomez-Gonzalez M, Hernandez J, Vidal P, Jurado F. Novel optimization algorithm for the power and energy management and component sizing applied to hybrid storage-based photovoltaic household-prosumers for the provision of complementarity services. J Power Sources 2021;482:228918.

[16] Lei M, Mohammadi M. Hybrid machine learning based energy policy and management in the renewable-based microgrids considering hybrid electric vehicle charging demand. Int J Electr Power Energy Syst 2021;128:106702.

[17] de la Torre S, Sanchez-Racero A, Aguado J, Reyes M, Martínez O. Optimal sizing of energy storage for regenerative braking in electric railway systems. IEEE Trans Power Syst 2015;30(3):1492-1500.

[18] Chen M, Wang M, Zhang D, Chen Y, Lu W. Improved coordinated control strategy for reliability enhancement of parallel PFCs with LCC restriction. IEEE Trans Transp Electrif 2022;8(2):2093-2105.

[19] Ju C, Wang P, Goel L, Xu Y. A two-layer energy management system for microgrids with hybrid energy storage considering degradation costs. IEEE Trans Smart Grid 2018;9(6):6047-6057.

[20] Luo P, Li Q, Zhou Y, Ma Q, Zhang Y, Peng Y, et al. Multi-application strategy based on railway static power conditioner with energy storage system. IEEE Trans Intell Transp Syst 2021;22(4):2140-2152.

[21] Coria G, Romero-Quete D, Romero A. Computational efficient approach to compute a prediction-of-use tariff for coordinating charging of plug-in electric vehicles under uncertainty. Int J Electr Power Energy Syst 2022;136:107692. http://doi.org/10.1016/j.ijepes.2021.107692.

[22] National Renewable Energy Laboratory Measurement and Instrumentation Data Center (MIDC). https://midcdmz.nrel.gov/; 2022 [accessed 1 July 2022].

[23] Electromagnetic Compatibility (EMC) - Limits - assessment of emission limits for the connection of unbalanced installations to MV HV and EHV power systems IEC/TR 61000-3-13 2008.

[24] Chen X, Wu W, Zhang B, Lin C. Data-driven DG capacity assessment method for active distribution networks. IEEE Trans Power Syst 2017;32(5): 3946-3957.

[25] Mirjalili S, Lewis A. The whale optimization algorithm. Adv Eng Software 2016;95:51-67.

[26] Zakeri B, Syri S. Electrical energy storage systems: A comparative life cycle cost analysis. Renew Sustain Energy Rev 2015;42:569–596.

[27] Yu X, Khambadkone AM. Reliability analysis and cost optimization of parallel-inverter system. IEEE Trans Ind Electron 2012;59(10):3881-3889.

[28] Chen Y, Chen M, Tian Z, Liu Y. Voltage unbalance management for high-speed railway considering the impact of large-scale DFIG-based wind farm. IEEE Trans Power Del 2020;35(4):1667-1677.

[29] Lofberg J. YALMIP: A toolbox for modeling and optimization in MATLAB. In Proceedings of the 2004 IEEE International Conference on Robotics and Automation 2004;284–289.

[30] Gurobi Optimization I. (2021). Gurobi optimizer reference manual. http://www.gurobi.com; 2021 [accessed 13 December 2021].

[31] Chen Y, Chen M, Liang Z, Liu L. Dynamic voltage unbalance constrained economic dispatch for electrified railways integrated energy storage. IEEE Trans Ind Inf 2022;18(11):8225-8235.